HHS Public Access

Author manuscript

J Toxicol Environ Health A. Author manuscript; available in PMC 2023 May 03.

Published in final edited form as:

J Toxicol Environ Health A. 2022 May 03; 85(9): 381–396. doi:10.1080/15287394.2021.2023716.

Implications of peroxisome proliferator-activated receptor gamma (PPARγ) with the intersection of organophosphate flame retardants and diet-induced obesity in adult mice

Gwyndolin M. Vail[1], **Sabrina N. Walley**[1], **Ali Yasrebi**[2], **Angela Maeng**[2], **Thomas J. Degroat**[3], **Kristie M. Conde**[4], **Troy A. Roepke**[1,2,3,4]

[1]Joint Graduate Program in Toxicology, Rutgers, The State University of New Jersey, Piscataway, NJ. USA

[2]Department of Animal Sciences, School of Environmental & Biological Sciences, Rutgers, The State University of New Jersey, New Brunswick, NJ. USA

[3]Graduate Program in Endocrinology and Animal Biosciences, School of Environmental & Biological Sciences, Rutgers, The State University of New Jersey, New Brunswick, NJ. USA

[4]Graduate Program in Neuroscience, Rutgers, The State University of New Jersey, Piscataway, NJ. USA

Abstract

Previously, organophosphate flame retardants (OPFRs) were demonstrated to dysregulate homeostatic parameters of energy regulation within an adult mouse model of diet-induced obesity (Vail et al. 2020). Using the same OPFR mixture consisting of 1 mg/kg/day of each triphenyl phosphate, tricresyl phosphate, and tris(1,3-dichloro-2-propyl)phosphate}, the current study examined the role of peroxisome proliferator-activated receptor gamma (PPARγ) in OPFR-induced disruption by utilizing mice with brain-specific deletion of PPARγ (PPARγKO) fed either a low-fat diet (LFD) or high-fat diet (HFD). Body weight and composition, feeding behavior, glucose and insulin tolerance, circulating peptide hormones, and expression of hypothalamic genes associated with energy homeostasis were recorded. When fed HFD, the effects of OPFR on body weight and feeding behavior observed in the previous wildtype (WT) study were absent in mice lacking neuronal PPARγ. This posits PPARγ as an important target for eliciting OPFR disruption in a diet-induced obesity model. Interestingly, female PPARγKO mice, but not males, experienced many novel OPFR effects not noted in WT mice, including decreased fat mass, altered feeding behavior and efficiency, improved insulin sensitivity and elevated plasma ghrelin and hypothalamic expression of its receptor. Taken together, these data suggest both direct roles for PPARγ in OPFR disruption of obese mice, and indirect sensitization of pathways alternative to PPARγ when neuronal expression is deleted.

Corresponding author: Troy A. Roepke, Ph.D., Department of Animal Sciences, School of Environmental and Biological Sciences, Rutgers, The State University of New Jersey, 84 Lipman Drive, Bartlett Hall, New Brunswick, NJ 08901, ta.roepke@rutgers.edu.

Declaration of Interest Statement

No potential competing interest was reported by the authors.

Keywords

flame retardants; metabolism; ingestive behavior; diet-induced obesity; PPARgamma

Introduction

Flame retardants (FRs) are a class of compounds that have become ubiquitous in use within common household and workplace products such as toys, furniture, most plastics, nail polish, and foodstuffs (Li et al. 2019; Peng et al. 2020; Yang et al. 2019; Young et al. 2018). Their intended use is to inhibit the flammability of the products these chemicals are imbedded within. However, because these compounds are not chemically bound, FRs may escape into the environment, where human exposure might occur through unintentional inhalation or ingestion (Wei et al. 2015). FRs were implicated as endocrine disrupting chemicals (EDCs). The endocrine system maintains various vital homeostatic functions and its disruption is associated with reprotoxic, neurotoxic, immunotoxin, and obesogenic outcomes (Barouki 2017). As a result of these consequences and due to the overwhelming prevalence of EDCs in the environment, the National Academy of Sciences (2019) acknowledged EDCs as significant risk to human health.

The current dominant class of FRs on the market are known as organophosphate flame retardants (OPFRs). OPFR prevalence rose simultaneously with the fall of FR predecessor polybrominated diphenyl ethers (PBDEs) after substantial toxicological evidence identified PBDEs as harmful EDCs, motivating regulatory actions (Zota et al. 2013; Israel Chemicals Ltd. 2015; Yasin et al. 2016; van der Veen and de Boer 2012). The overwhelming usage of OPFRs has led to increased human exposure, resulting in detection of these chemicals within human serum (680-709 ng/ml), breast milk (1-10 ng/ml), and urine (1-10 ng/ml) samples (Butt et al. 2014; Hoffman et al. 2017; Ma et al. 2017; 2019; Meeker et al. 2013). Subsequent research into the safety of these chemicals revealed similar EDC capacity to their PBDE predecessors (Dishaw et al. 2011; Patisaul et al. 2013; Kylie et al. 2018; Belcher et al. 2014; Pillai et al. 2014; Liu et al. 2012; 2013; Hu et al. 2019; Steves et al. 2018; National Academy of Sciences 2019).

EDC action by OPFRs may be attributed to their capacity to interact with nuclear receptors such as estrogen receptor alpha (ERα) or peroxisome proliferator-activated receptor gamma (PPARγ) (Ji et al. 2020; Kojima et al. 2013; National Academy of Sciences 2019; Pillali et al. 2014; Tung et al. 2017). Three of the most commonly used OPFRs that demonstrate these receptor interactions are triphenyl phosphate (TPP), tris(1,3-dichloro-2-proply)phosphate (TDCPP), and tricresyl phosphate (TCP) and as such, these three OPFRs were selected for the current study investigating the specific role of PPARγ as a target for OPFR dysregulation of ingestive behaviors and energy homeostasis. EDC impairment of energy homeostasis presents as a significant human health concern because it may predispose individuals to developing metabolic syndrome and its symptomatic sequelae obesity, hypertension, inflammation and pre-diabetes (Hevener et al; 2015; Kobos et al 2020; Dabass et al 2018).

PPARγ is peripherally dominant within adipose tissues, where it directs adipogenesis and lipid metabolism (Wang 2010). Disordered fatty acid metabolism and storage is

associated with insulin resistance, and one of the leading pharmacological therapies are thiazolidinediones (TZDs), which are potent PPAR agonists (Wang 2010). Adipocyte PPARγ is postulated to be the major target for TZD action, however Lu et al. (2011) observed that brain-specific knockout of PPARγ (PPARγKO) abolished the effects of TDZ rosiglitazone.

PPARγ is expressed within subpopulations of neurons termed neuropeptide Y (NPY) and proopiomelanocortin (POMC) neurons within the arcuate (ARC) nucleus of the hypothalamus. These neurons act as integral central regulators of ingestive behavior and energy expenditure (Garretson et al. 2015; Sarruf et al. 2009). Highlighting the importance of PPARγ in these pathways, Garretson et al (2015) reported that centrally administered rosiglitazone induced ingesting and hoarding behaviors in male mice and hamsters that is abolished with targeted knockout of PPARγ within POMC neurons (Stump et al. 2016). In addition, brain-specific PPARγKO mice also exhibit resistance to diet-induced obesity (Lu et al. 2011).

Previously, Vail et al (2020) demonstrated that sub-chronic OPFR exposure within adult mice produced alterations in feeding behavior and energy homeostasis that were gender-dependent. These effects intersected with diet-induced obesity, exacerbating the effects of ingesting a high fat diet (HFD) to gain weight and fat tissue. In addition, while no marked alterations in body weight were noted in OPFR-exposed females, these animals ate less food and initiated fewer HFD meals per day (Vail et al. 2020). Because PPARγ is a known OPFR target, and because PPARγ is integrated in central regulation of ingestive behavior and energy homeostasis, it was postulated that the dysregulated energy homeostasis observed by Vail et al. (2020) may partially be due to OPFR action on neuronal PPARγ. To this end, the current study exposed neuronal-specific PPARγ knockout transgenic mice to OPFRs concurrently with administration of either LFD or HFD.

Materials and Methods

Animals

All animal experiments followed National Institution of Health standards and were conducted with approval by the Rutgers University Institutional Animal Care and Use Committee. Male *Pparg*$^{fl/fl}$ mice and female *Syn1*$^{Cre/+}$ mice were purchased from Jackson Laboratories and bred to generate *Pparg*$^{fl/+}$/*Syn1*$^{Cre/+}$ offspring. Female *Pparg*$^{fl/+}$/*Syn1*$^{Cre/+}$ offspring were subsequentially bred with *Pparg*$^{fl/fl}$ male mice to generate *Pparg*$^{fl/fl}$/*Syn1*$^{Cre/+}$ transgenic knockout mice lacking PPARγ only within the brain (PPARγKO). Because *Syn1-cre* expresses within the testis and male Syn1-cre mice are capable of producing confounding germline recombinants (Rempe et al. 2006), the *Syn1-cre* allele were maintained within female breeders, which did not experience this effect. Mice were maintained under controlled temperature (23°C) and photoperiod conditions (12/12 hr light/dark cycle) and fed food and water *ad libitum*. At weaning, animals were number-tagged and ear-clipped for genotyping and started on a standard low-phytoestrogen chow diet (Lab Diets 5V75) until the start of experimentation at 10 weeks of age.

Genotyping

Initial genotyping used DNA samples from ear clippings taken at weaning, and after experimental completion, ear samples were again taken post-euthanasia to confirm the animal was the correct genotype. Genotyping for PPARγKO mice required testing for the presence of both *Syn1-cre* and the absence of *Pparg*. To this end, primers were used according to established protocols from Jackson Laboratory (Syn1-Cre+: XXXF: CTCAGCGCTGCCTCAGTCT, XXXR: GCATCGACCGGTAATGCA; and Syn1-Cre-: XXXF: CTAGGCCACAGAATTGAAAGATCT, XXXR: GTAGGTGGAAATTCTAGCATCATCC) to detect for heterozygosity of the *Syn1-cre* gene. Primers (XXXF: TGGCTTCCAGTGCATAAGTT, XXXR: TGTAATGGAAGGGCAAAAGG) were then utilized to detect homozygous absence of *Pparg*. Ear-clip DNA was extracted and *Syn1*-cre was amplified in RedTaq mix (Sigma) with 9 cycles of 94°C for 20 sec, 65°C for 15 sec, 68°C for 10 sec, followed by another 9 cycles of 94°C for 15 sec, 60°C for 15 sec, 72°C for 10sec 68°C for 10 sec, and lastly 27 cycles of 94°C for 15 sec, 60°C for 15 sec, 72°C for 10 sec. *Pparg* DNA was amplified with the same temperature protocol, but repeated the first two cycles 15 times, and repeated the last cycle 44 times. Amplified DNA was then loaded into wells of 3% agarose gel in 1x TBE buffer for DNA electrophoresis separation and genotype identification.

Diets

Starting at 10 weeks old, PPARγKO mice were switched from standard lab chow to either a low-fat diet (LFD, 3.85 kcal/g, 10% fat, 20% protein, 70% carbohydrate; D12450H) or high-fat diet (HFD, 4.73 kcal/g, 45% fat, 20% protein, 35% carbohydrate; D12451; Research Diets) to generate a model for diet-induced obesity.

OPFR Dosing

Since human exposure to EDCs such as OPFRs is mixed, three common OPFRs were used in a singular mixture for this study. OPFRs utilized were tricresyl phosphate (TCP, CAS no. 1330-78-5; purity 99%; purchased from AccuStandard, New Haven, CT), and triphenyl phosphate (TPP, CAS no. 115-86-6; purity 99%) and tris (1,3-dichloro-2-propyl)phosphate (TDCPP, CAS no. 13674-87-8; purity 95.6%) (both purchased from Sigma-Aldrich, St. Louis, MO). One hundred mg of each OPFR were dissolved as a singular mixture within a total of 1 ml acetone (Sigma) to generate 1 mg/ml stock mixture of OPFR-acetone for long-term storage. A working solution was then made by transferring 100 μl OPFR-acetone into 10 ml sesame oil (Sigma-Aldrich) to create an oil mixture containing 1 mg/ml OPFR (OPFR-oil). To generate the control-oil mixture, 100 μl acetone was added to 10 ml sesame oil (control-oil). OPFR-oil and control-oil mixtures were left stirring for 48-72 hr to evaporate the acetone from the mixture. OPFR-oil or control-oil were then added to the minimal amount of dehydrated peanut butter (approximately 50 mg) to create an appetizing rehydrated peanut butter mixture with a final concentration of 1 mg/kg bw OPFR or equivalent amount of OPFR-free rehydrated peanut butter. The resulting doses were supplied to mice daily to be consumed orally. Oral exposure began at 10 weeks of age at 0900-1100 hr each day for a total of approximately 7 weeks.

Experimental Design

Starting at 10 weeks of age, adult male and female mice (n = 8 per gender, per diet, per treatment) were weight-matched in paired housing, supplied either LFD or HFD, and were given daily oral doses of OPFR-oil or control-oil for the entirety of the 7-week experimental timeline. Baseline body composition (fat and lean mass) were quantified by EchoMRI™ Body composition (Houston, TX) on the first day of dosing, and then again after 4 weeks of treatment with OPFR-oil or control-oil mixtures. Body weight and crude food intake per cage were measured weekly. After 4 weeks of exposure, mice were transferred to the Biological Data Acquisition (BioDAQ, Research Diets, New Brunswick, NJ) chambers for a total of 1 week. Mice were single-housed during this time and dosed with OPFR-oil or control-oil the same as when pair-housed. Mice underwent 94 hr habituation and then 72 hr data acquisition for feeding behaviors (meal size, duration, frequency). In the BioDAQ system, LFD or HFD were placed in hoppers that measured food intake as decreased chow weight within the hopper. These hoppers were touch-sensitive and whenever the hopper was accessed by the mouse for food, the software flagged that action as a “bout”. A bout marked the start of a “meal” if it was the first bout to occur within 300 sec. A meal could consist of any number of bouts and lasted until 300 sec passed after the last bout. The next bout recorded would then indicate the start of a new meal. Some mice fed HFD exhibited what is to be referred to as “food chewing” behavior, where chow was removed from the hopper but employed for enrichment chewing, and not actually consumed. This behavior could not be accounted for in statistical analysis of ingestive behavior and therefore necessitated the exclusion of data when the behavior was observed. This accounts for the variation in n within the feeding behavior data. During the last week of exposure, all mice were tested for glucose and insulin tolerance. To ensure equivalent basal glucose levels, mice were fasted for 5 hr before the glucose tolerance test (GTT). A bolus of 2 g/kg glucose was then given by intraperitoneal (ip) injection and resulting blood-glucose was measured from tail bleeds using an AlphaTrak glucometer (Zoetis, Parsippany, NJ) at 0, 15, 30, 60, 90, and 120-min post-injection. Mice were given a 4-day recovery period before undergoing the insulin tolerance test (ITT). After a 4 hr fast, mice were IP injected with 0.75 U/kg insulin and blood-glucose was recorded from tail bleeds at 0, 15, 30, 60, 90, and 120 min. OPFR- or control-oil dosing was continued throughout these experimentations, and up through the day of euthanization, occurring approximately 1 week after the ITT. On this day, mice were dosed at 0900 hr, fasted at 1000 hr, and then euthanized at 1100 hr by decapitation under sedation with 100 mg/ml ketamine. Female mice were euthanized during diestrus, as determined by vaginal cytology, to control for circulating ovarian hormone levels. Terminal trunk blood was collected in K^+-EDTA coated tubes with the addition of proteinase inhibitor 4-(2-aminoethyl) benzene sulfonyl fluoride hydrochloride (1 mg/ml, Sigma-Aldrich) to reduce peptide degradation. Samples were chilled on ice until centrifugation at 1,100 g for 15 min at 4°C. Plasma supernatant was then collected and stored at −80°C for later analysis of insulin, leptin, and ghrelin levels using a multiplex assay (MMHMAG-44 K, EMD Millipore, Billerica, MA). In addition, microdissection samples from the arcuate nucleus of the hypothalamus were collected and stored at −80°C for later RNA extraction and conversion to cDNA in preparation for gene expression quantification according to Yasrebi et al. (2016). A graphical depiction of the experimental outline is summarized in Figure 1.

Real-time Quantitative PCR

All primers for real-time polymerase chain reaction quantification (rt-qPCR) were designed to span exon-exon junctions using Clone Manager 5 software (Sci Ed Software, Cary, NC) and synthesized by Life Technologies and are listed in Table 1. Amplification of 4 μL ARC cDNA was conducted by a CFX-Connect Real-time PCR instrument (BioRad, Hercules, CA) using either PowerSYBR Green master mix (Life Technologies) or SsoAdvanced SYBR Green (BioRad). Amplification of all genes used the following protocol: initial denaturing at 95°C for 10 min (PowerSYBR) or 3 min (SsoAdvanced) followed by 40-45 cycles of amplification by alternating 10 sec of denaturing at 94°C and 45 sec of annealing at 60°C. A final dissociation step was incorporated for melting point analysis by 60 cycles of 95°C for 10 sec, 65°C to 95°C (stepping 0.5°C increments each cycle) for 5 sec, and 95°C for 5 sec. Standard curves for each primer pair were generated using serial dilutions of basal hypothalamic cDNA in triplicate to determine efficiency [$E = 10(^{-1/m})-1$, m = slope] of each primer pair and are denoted in Table 1.

Reference genes used for target gene comparison were *Actb* (β-actin), *Gapdh* (glyceraldehyde-3-phosphate dehydrogenase), and *Hprt* (Hypoxanthine-guanine phosphoribosyltransferase). Diluted (1:20) basal hypothalamic (BH) cDNA from an untreated, intact wild-type male was employed as a positive control. Negative controls consisted of a water blank and a BH RNA sample that lacked the enzyme needed to convert it to cDNA. Quantification data were excluded if the sample did not show a single product at the expected melting point. All gene expression data were calculated using the geometric mean of the reference genes *Actb*, *Gapdh*, and *Hprt*. Relative mRNA expression data were then analyzed using the $\Delta\Delta C_q$ method, normalizing to control-LFD samples (Livak and Schmittgen 2001; Pfaffl 2001; Schmittgen and Livak 2008).

Data Analysis

All data are depicted as mean ± SEM. Data were analyzed using either GraphPad Prism software (GraphPad Software, LA Jolla, CA) by a two-way ANOVA (OPFR and Diet) with a *post-hoc* Newman-Keul's multiple comparisons test, or with Statistica 7.1 software (StatSoft, Tulsa, OK, USA) using both multi-factorial ANOVA with repeated-measures and a three-way ANOVA (Diet, OPFR, Time), followed with *post-hoc* Newman-Keul's multiple comparisons test. Effects were considered significant at $P \leq 0.05$.

Results

Physiological Parameters

Beginning at 10 weeks of age, mice received either control-oil or OPFR-oil mixture (1 mg/kg each of TCP, TPP, and TDCPP). For the first 4 weeks, body weight and crude food intake were measured weekly. Feeding efficiency was calculated as the ratio of bodyweight gain to crude food intake and is represented as grams gained to kcal consumed. Body composition of lean and fat mass were assessed by EchoMRI™ (Figures 2-3) on dosing day one (baseline) and after 4 weeks of dosing. Baseline bodyweights were taken at day zero, just prior to treatment and diet initiation (males: control − 24.6 ± 0.7 g, OPFR − 24.5 ± 0.3 g; females: control − 19.9 ± 0.4 g, OPFR − 19.4 ± 0.3 g).

PPARγKO males did not appear to be affected by OPFR exposure within these parameters (Figure 2). However, HFD significantly augmented bodyweight gain in females only within OPFR-treated animals (Figure 3A). This appears to be attributed to a reduction in LFD weight-gain, supported by a 3-fold decrease in LFD feeding efficiency in female mice exposed to OPFR compared to control (Figure 3C). Further, while control females displayed a typical elevated fat mass ratio from consuming high fat chow (Figure 3D), fat mass was identical in LFD- and HFD-fed animals treated with OPFR. *Post-hoc* analysis revealed this finding was resulted from a 5 ± 2% fall in fat mass in OPFR exposed, HFD females compared to HFD-fed controls (Figure 3D). Data demonstrated that OPFR exposure was impairing the process of fat accumulation by consuming HFD chow, represented in the statistical interaction between diet and OPFR exposure (Figure 3D). This has interesting implications for the specific role of neuronal PPARγ in protecting against OPFR-induced dysregulation of adipogenesis.

Feeding Behaviors

OPFR exposure induced subtle alterations to hourly food intake in PPARγKO male mice (Figure 4A). During 2100-2200 hr, OPFR-exposed males consumed more LFD than their controls (Figure 4A). During the same window, OPFR exposed mice consumed more LFD than HFD (Figure 4A), whereas control mice did not experience this diet effect. Control males consumed more LFD than HFD during 2200-2300 hr (Figure 4A). However, total food intake over 96 hr was not affected, as was meal size and frequency (Figure 4B, 4C, 4E). While control males fed HFD spent less time in their meals compared to LFD counterparts (Figure 4D), this diet effect was not found in OPFR-treated mice, indicating an OPFR influence on meal duration. PPARγKO females also experienced a main effect of OPFR on hourly food intake patterns (Figure 5A). *Post*-hoc analysis revealed specific alterations during the night. During 2100-2200 hr and during 2300-2400 hr, OPFR diminished LFD intake compared to oil-control females (Figure 5A). HFD intake was also decreased by OPFR during 1900-2000 hr and 0200-0300 hr (Figure 5A). Conversely, a significant spike in HFD consumption occurred during 0400-0500 hr in OPFR-exposed females. Unfortunately, due to an issue with excessive food chewing behavior, where chow removed from the hopper was not consumed and instead used for chewing enrichment, the BioDAQ™ apparatus was not able to accurately measure total HFD intake over the 96-hr period. Animals fed LFD did not have this issue, and OPFR exposure was found to exert no significant effect on total ingestion (Figure 5B). In addition, OPFR did not markedly alter meal duration or size (Figure 5D, 5E). Control females ingested more meals per day when fed HFD as compared to LFD (Figure 5C), but OPFR exposure eliminated the statistical difference between diets (Figure 5C).

Glucose and Insulin Tolerance

Control PPARγKO male mice exhibited a HFD-induced elevation of fasting glucose (Figure 6A). Male mice exposed to OPFR, however, displayed equivalent LFD and HFD fasting glucose levels. This is explained by an OPFR-induced elevation of fasting glucose in male mice fed LFD (Figure 6A). Further, OPFR exposure also resulted in increased blood-glucose in mice fed HFD at two time points during the glucose tolerance test (Figure 6B). This correlated to OPFR-treated males displaying greater AUC in HFD-fed than LFD-fed mice

(Figure 6C). This diet effect was not detected in control males, therefore OPFR may be diminishing the ability of PPARγKO males to respond to sudden changes in glucose homeostasis. In female mice, HFD elevated fasting glucose, irrespective of treatment (Figure 6D). There were no OPFR, or diet effects on glucose tolerance.

Insulin tolerance AUC was unaltered by diet or OPFR in PPARγKO males (Figure 17B). OPFR enhanced the response to insulin in male mice fed HFD at t = 15 min (Figure 7A), such that the response was identical to that noted in LFD-fed animals. Further, while control males fed HFD exhibited a reduced response to insulin at the same time point (Figure 7A), OPFR-exposed males showed no marked effect of diet at any time points. Data indicate that OPFR treatment eliminated the effect of HFD to lower insulin sensitivity in PPARγKO males. In females, OPFR exposure resulted in reduced blood-glucose at multiple time points throughout the insulin tolerance test (Figure 7C). This resulted in a significant reduction of AUC in OPFR-treated females fed LFD compared to HFD (Figure 7D). Overall, data suggests that OPFR increased insulin sensitivity in PPARγKO females fed LFD.

Peptide Hormones

Terminal plasma hormone levels analyzed for leptin, insulin, and ghrelin. PPARγKO male mice demonstrated no marked effect due to OPFR exposure (Figure 8A-8C). The only significant effect reported in males was that HFD induced an overall effect to elevate circulating leptin levels (Figure 8B). Female PPARγKO mice, however, displayed more interesting results. Leptin levels were increased by HFD (Figure 8E), but *post-hoc* testing only revealed a significant effect of diet in control mice (Figure 8E); there was no significant difference between LFD and HFD leptin levels in OPFR-exposed females. This may be attributed to a significant repression of circulating leptin by OPFR in HFD-fed animals (Figure 8E) and highlights the interaction of OPFR exposure and diet-induced alterations to leptin signaling (Figure 8E). Further, this effect is in agreement with the insulin results (Figure 8D). Whereas the significant effect of diet (Figure 8D) is represented in *post-hoc* significance between LFD- and HFD-fed controls, there was no significant difference found in the OPFR-treated group. Finally, the inverse was found for the orexigenic hormone ghrelin (Figure 8F). An overall diet effect was also noted with HFD reducing circulating ghrelin (Figure 8F), but this period of OPFR exposure was shown to exacerbate the effect of diet by significantly increasing the levels of ghrelin in LFD-fed females (Figure 8F). This led to a significant difference between diets (Figure 8F) only within the OPFR-treated mice. Taken together, it appears that female PPARγKO mice may be more susceptible to OPFR disruption of plasma hormones than their male counterparts. Further, OPFR exposure was found to interact with diet by reducing the typical rise of anorexigenic insulin and leptin in the blood in response to a high fat diet, while also increasing plasma levels of orexigenic ghrelin when fed a LFD.

Arcuate (ARC) Gene Expression

ARC microdissections were analyzed for important ARC neuropeptide transcripts governing energy homeostasis *Npy*, *Agrp*, *Pomc*, and *Cart*, as well as *Ers1* (ERα) expression and ARC receptors for insulin (*Insr*), leptin (*Lepr*), and ghrelin (*Ghsr*). The only direct effect of OPFR within PPARγKO mice is reported in female mice fed LFD, which experienced

a nearly 30% reduction in *Ghsr* expression. In addition, an overall significant effect of OPFR to lower *Ghsr* expression in females was noted in the ANOVA analysis (Table 2). In male mice, *Agrp* expression was significantly diminished by HFD (Table 2). While this was represented in *post-hoc* significance between LFD- and HFD-fed control males (Table 2), there was no significant effect of diet within OPFR-exposed males. This indicates a possible effect of OPFR exposure to inhibit the impact that diet has on *Agrp* expression in the ARC. These observations, or any others similar to it, were not seen in female PPARγKO mice. A few diet effects are also reported in PPARγKO males for decreased expression of *Npy* and elevated *Cart* (Table 2). Diet effects were also observed in females. Both *Agrp* and *Npy* ARC expression were diminished by HFD (Table 2), and additionally returned *post-hoc* significance between diets for both treatment groups (Table 2).

Discussion

Since human exposure to environmental toxicants is not limited to sensitive developmental periods, it is also important to understand how exposure to chemicals like OPFRs may affect endocrine signaling during adult life. PPARγ is a lesser studied target of OPFRs, and this study aimed to help address gaps in understanding its role in OPFR-induced endocrine disruption. This discussion heavily references our previous study in wildtype mice using the same OPFR exposure and methodology (Vail et al. 2020) as a comparison tool for examining differential effects of OPFR exposure when PPARγ is absent in the brain. It is understood that the need to reference previous research is a significant limitation of this study, therefore a table summarizing the direct effects of OPFR exposure in the wildtype (WT) study and the KO study is provided to help visualize the conclusions drawn from the current data (Table 3).

Neuronal knockout of PPARγ has previously been noted to limit the rise in weight gain seen in mice fed HFD (Lu et al. 2011), and our findings reported similar trends of an approximate 10% less weight gain in HFD-fed PPARγKO mice than WT counterparts (Vail et al. 2020). PPARγKO males were not directly affected by OPFR exposure with respect to weight gain or adiposity. However, in WT mice, OPFR-treated males experienced greater weight gain and fat mass than control when fed HFD (Vail et al. 2020). Therefore, it is conceivable that OPFR-induced adiposity and weight gain in males might be attributed, in part, to interaction with PPARγ. PPARγ is well-known for its endogenous regulation of adipose tissue and lipid metabolism (Janani and Ranjitha Kumari 2015; Wang 2010). Therefore, it follows that OPFR disruption of PPARγ might manifest as dysregulated fat accumulation.

Whereas WT females displayed no marked effects of OPFRs on bodyweight nor body composition (Vail et al. 2020), HFD-fed PPARγKO females exposed to OPFR exhibited decreased fat mass compared to their control-treated counterparts. This represents an interaction of genotype and OPFR, whereas the loss of neuronal PPARγ sensitizes mice to OPFR action on fat deposition. Further, control-treated PPARγKO females demonstrated roughly 5-fold greater feeding efficiency than WT animals reported by Vail et al. (2020), indicating females lacking neuronal PPARγ more readily translate energy intake into bodyweight. Evidence indicates the importance of neuronal PPARγ in regulating adipose homeostasis. Interestingly, OPFR treatment eliminated this genotype effect, reducing

PPARγKO LFD feeding efficiency to that seen in WT females (Vail et al. 2020). In addition, OPFR exposure diminished circulating leptin in HFD-fed females. Adipose tissue is a large source of leptin production and correlates with reduced fat mass in female PPARγKO mice. One possible explanation for these novel effects of OPFR is that the loss of neuronal PPARγ targets may be shifting central actions of OPFR onto other targets, such as estrogenic pathways. If this were the case, and if OPFR is acting agonistically, this may result in the observed decrease in adiposity and feeding efficiency in PPARγKO mice. Another hypothesis may be that without neuronal PPARγ, OPFR is acting to a higher degree on peripheral PPARγ, which directly controls adipose tissue homeostasis. This hypothesis is weakened, though, by the knowledge that brain knockout of PPARγ does not result in altered peripheral PPARγ expression (Fernandez et al. 2017; Lu et al. 2011). With many unknown variables, it is not possible to conclude with certainty the exact mechanisms underlying these findings.

Feeding behavior in both WT and PPARγKO male mice appears to be unaffected by OPFR treatment. However, while OPFR exposure to WT females fed is reported to diminish meal frequency and total food intake (Vail et al. 2020), these effects were absent in PPARγKO females. Data demonstrate that the effect of OPFR to reduce feeding initiation is in part, through neuronal PPARγ interaction. OPFR-treatment in PPARγKO mice also resulted in disrupted hourly feeding patterns. WT females were largely unaffected by OPFR treatment excepting minor time-specific differences (Vail et al. 2020). Again, this presents as a novel effect of OPFRs in the absence of neuronal PPARγ.

In WT mice, HFD conferred typical impaired glucose tolerance, and was unaltered by OPFR exposure (Vail et al. 2020). However, in control PPARγKO mice, glucose tolerance was unaffected by diet. This presents as a genotypic effect indicating that neuronal PPARγ is important in conferring impaired glucose sensitivity due to diet-induced obesity. This effect was also observed by Lu et al. (2012), but is in contrast to Fernandez et al (2017), who showed identical tolerance curves between WT and brain-PPARγKO mice fed HFD. Regardless, pertaining to OPFR exposure, our current study found that OPFR treatment restored HFD-induced impairment of glucose tolerance in male PPARγKO mice. This implies that OPFRs may be acting on targets alternative to brain PPARγ to mimic the role PPARγ plays in regulating glucose tolerance. Glucose tolerance in female mice was unaffected by OPFR exposure.

Neuronal knockout of PPARγ also impacts insulin tolerance. Insulin tolerance is impaired by HFD in WT mice (Vail et al. 2020), but no significant change in AUC was observed in control PPARγKO mice. This was suggested to be a genotypic effect and signifies an important role for neuronal PPARγ in development of HFD-induced insulin intolerance. Interestingly, male PPARγKO mice were further protected against HFD-insulin intolerance when exposed to OPFR, displaying identical insulin tolerance curves and AUC whether fed LFD or HFD. In contrast to males, female PPARγKO mice experienced a marked reduction in insulin tolerance when fed LFD. Overall, OPFR exposure appears to sensitize male and female mice to insulin on HFD and LFD, respectively. While the mechanistic aspect of these results remains indiscernible without further investigations, it is conceivable that the loss of neuronal PPARγ as an OPFR target may enhance OPFR action on other pathways

that govern glucose homeostasis, resulting in our observed findings. POMC neurons within the ARC are essential regulators of hepatic glucose production (Caron et al. 2018; Shi et al. 2013) and are reported to be impacted by OPFR exposure, increasing excitability and pre-synaptic input (Vail and Roepke 2020). Importantly, these neurons also express PPARγ, and selective knockout of POMC-PPARγ was demonstrated to improve glucose metabolism and reduce body weight, fat mass, and food intake when fed HFD (Long et al. 2014). Glucose homeostasis was also impacted within brain-specific PPARγKO mice (Figures 6 and 7), indicating that the loss of neuronal PPARγ may further expose ARC control of energy homeostasis to OPFR-mediated disruption.

Generally, our experimentations with brain-specific PPARγKO animals revealed that when fed HFD, the effects of OPFR on increased bodyweight and fat mass and altered feeding behavior reported in WT mice were not present in mice lacking neuronal PPARγ. Data suggested that PPARγ is required for OPFR exposure to impact the effects of diet-induced obesity. Conversely, multiple novel effects of OPFR exposure were reported in female, but not male, PPARγKO mice fed LFD (refer to Table 3). Collectively, data signify an intriguing direct role of PPARγ in EDC actions of OPFRs in a model of diet-induced obesity, and a simultaneous indirect sensitization of alternative, perhaps compensatory pathways when neuronal PPARγ is absent in non-obese female mice.

Conclusions

Overall, this study provides evidence of PPARγ involvement in EDC actions of three common OPFRs. It is important to understand the mechanisms of OPFR EDC action because dysregulation of endocrine functions governing energy homeostasis may pre-dispose individuals to metabolic issues such as obesity, diabetes, and metabolic syndrome. Further examination of the toxicological potential of OPFRs might benefit from investigating the role of PPARγ in specific neuronal populations such as POMC neurons, perhaps by utilizing transgenic mice with selective knockout of PPARγ only within POMC neurons.

The main objective of toxicological studies is to provide data needed in order to determine the risk involved in exposure. While future studies into mechanistic actions of OPFRs on POMC or other hypothalamic neurons may certainly be intriguing and informative, there is already a significant body of evidence highlighting the hazards of permitting the widespread exposure of human populations to organophosphate flame retardants.

Acknowledgements

This work was supported by the US Department of Agriculture–National Institute of Food and Agriculture (NJ06195, TAR) and the National Institutes of Health (R21ES027119, R01MH123544, and P30ES005022, TAR). SNW was funded by R21ES027119-S1 and GMV was funded, in part, by T32ES007148.

Data Availability Statement

The data that support the findings of this study are available from the corresponding author, T.A. Roepke, upon reasonable request.

References

Barouki R 2017. Endocrine disruptors: Revisiting concepts and dogma in toxicology. Comptes Rendus Biol. 340: 410–413.

Belcher SM, Cookman CJ, Patisaul HB, and Stapleton HM. 2014. In vitro assessment of human nuclear hormone receptor activity and cytotoxicity of the flame retardant mixture FM 550 and its triarylphosphate and brominated components. Toxicol Lett 228:93–102. [PubMed: 24786373]

Butt CM, Congleton J, Hoffman K, Fang M, and Stapleton HM. 2014. Metabolites of organophosphate flame retardants and 2-ethylhexyl tetrabromobenzoate in urine from paired mothers and toddlers. Environ Sci Technol 48 :10432–10438. [PubMed: 25090580]

Caron A, Lemko HMD, Castorena CM, Fujikawa T, Lee S, Lord CC, Ahmed N, Lee CE, Holland WL, Liu C, and Elmquist JK. 2018. POMC neurons expressing leptin receptors coordinate metabolic responses to fasting via suppression of leptin levels. eLife 7: e33710. [PubMed: 29528284]

Dabass A, Talbott EO, Rager JR, Marsh GM, Venkat A, Holguin F, and Sharma RK. 2018. Systemic inflammatory markers associated with cardiovascular disease and acute and chronic exposure to fine particulate matter air pollution ($PM_{2.5}$) among US NHANES adults with metabolic syndrome. Environ Res 161:485–491. [PubMed: 29223110]

Dishaw LV, Powers CM, Ryde IT, Roberts SC, Seidler FJ, Slotkin TA, and Stapleton HM. 2011. Is the PentaBDE replacement, tris (1,3-dichloro-2-propyl) phosphate (TDCPP), a developmental neurotoxicant? Studies in PC12 cells. Toxicol Appl Pharmacol 256: 281–289. [PubMed: 21255595]

Fernandez MO, Sharma S, Kim S, Rickert E, Hsueh K, Hwang V, Olefsky JM, and Webster NJG. 2017. Obese neuronal PPARγ knockout mice are leptin sensitive but show impaired glucose tolerance and fertility. Endocrinology 158:121–133. [PubMed: 27841948]

Garretson JT, Teubner BJ, Grove KL, Vazdarjanova A, Ryu V, and Bartness TJ. 2015. Peroxisome proliferator-activated receptor gamma controls ingestive behavior, agouti-related protein, and neuropeptide Y mRNA in the arcuate hypothalamus. J Neurosci 35 :4571–4581 [PubMed: 25788674]

Hevener AL, Clegg DJ, and Mauvais-Jarvis F 2015. Impaired estrogen receptor action in the pathogenesis of the metabolic syndrome. Mol Cell Endocrinol 418:306–321. [PubMed: 26033249]

Hoffman K, Butt CM, Webster TF, Preston EV, Hammel SC, Makey C, Lorenzo AM, Cooper EM, Carignan C, Meeker JD, Hauser R, Soubry A, Murphy SK, Price TM, Hoyo C, Mendelsohn E, Congleton J, Daniels JL, and Stapleton HM. 2017. Temporal trends in exposure to organophosphate flame retardants in the United States. Environ Sci Technol Lett 4:112–118. [PubMed: 28317001]

Hu W, Jia Y, Kang Q, Peng H, Ma H, Zhang S, Hiromori Y, Kimura T, Nakanishi T, Zheng L, Qiu Y, Zhang Z, Wan Y, and Hu J. 2019. Screening of ouse Ddust from Chinese homes for chemicals with liver X receptors binding activities and characterization of atherosclerotic activity using an *in vitro* macrophage cell line and ApoE−/− mice. Environ Health Perspect 127:117003–117003. [PubMed: 31724879]

Israel Chemicals ltd. 2015. Worldwide flame retardants market to reach 2.8 million tonnes in 2018. Addit Polymers 2015:11.

Janani C, and Ranjitha Kumari BD. 2015. PPAR gamma gene – A review. Diabetes Metab Syndrome: Clin Res Rev 9: 46–50.

Ji X, Li N, Ma M, Rao K, and Wang Z. 2020. *In vitro* estrogen-disrupting effects of organophosphate flame retardants. Sci Total Environ 727:138484. [PubMed: 32330712]

Kobos L, Alqahtani S, Xia L, Coltellino V, Kishman R, McIlrath D, Perez-Torres C, and Shannahan. 2020. Comparison of silver nanoparticle-induced inflammatory responses between healthy and metabolic syndrome mouse models. J Toxicol Environ Health A 83: 249–268. [PubMed: 32281499]

Kojima H, Takeuchi S, Itoh T, Iida M, Kobayashi S, and Yoshida T. 2013. *In vitro* endocrine disruption potential of organophosphate flame retardants via human nuclear receptors. Toxicology 314: 76–83. [PubMed: 24051214]

Kylie DR, Horman B, Phillips LA, McRitchie LS, Watson S , Deese-Spruill J, Jima D, Sumner S, Stapleton MH, and Patisaul BH. 2018. EDC IMPACT: Molecular effects of developmental FM

550 exposure in Wistar rat placenta and fetal forebrain. Endocr Connect 7: 305–324. [PubMed: 29351906]

Li J, Zhao L, Letcher RJ, Zhang Y, Jian K, Zhang J, and Su G. 2019. A review organophosphate Ester (OPE) flame retardants and plasticizers in foodstuffs: Levels, distribution, human dietary exposure, and future directions. Environ Int 127:35–51 [PubMed: 30901640]

Liu X, Ji K, and Choi K. 2012. Endocrine disruption potentials of organophosphate flame retardants and related mechanisms in H295R and MVLN cell lines and in zebrafish. Aquat Toxicol 114-115:173–181. [PubMed: 22446829]

Liu X, Ji K, Jo A, Moon HB, and Choi K. 2013. Effects of TDCPP or TPP on gene transcriptions and hormones of HPG axis, and their consequences on reproduction in adult zebrafish (*Danio rerio*). Aquat Toxicol 134-135: 104–111. [PubMed: 23603146]

Livak KJ and Schmittgen TD. 2001.Analysis of relative gene expression data using real-time quantitative PCR and the 2(-Delta Delta C(T)) method. Methods. 25:402–408. [PubMed: 11846609]

Long L, Toda C, Jeong JK, Horvath TL, and Diano S. 2014. PPARgamma ablation sensitizes proopiomelanocortin neurons to leptin during high-fat feeding. J Clin Invest 124: 4017–4027. [PubMed: 25083994]

Lu M, Sarruf DA, Talukdar S, Sharma S, Li P, Bandyopadhyay G, Nalbandian S, Fan WQ, Gayen JR, Mahata SK, Webster NJ, Schwartz MW, and Olefsky JM. 2011. Brain PPAR-γ promotes obesity and is required for the insulin-sensitizing effect of thiazolidinediones. Nature Med 17:618–622. [PubMed: 21532596]

Ma J, Zhu H, and Kannan K. 2019. Organophosphorus flame retardants and plasticizers in breast milk from the United States. Environ Sci Technol Lett 6:525–531. [PubMed: 31534982]

Ma Y, Jin J, Li P, Xu M, Sun Y, Wang Y, and Yuan H. 2017. Organophosphate ester flame retardant concentrations and distributions in serum from inhabitants of Shandong, China, and changes between 2011 and 2015. Environ Toxicol Chem 36:414–421. [PubMed: 27391075]

Meeker JD, Cooper EM, Stapleton HM, and Hauser R. 2013. Urinary metabolites of organophosphate flame retardants: temporal variability and correlations with house dust concentrations. Environ Health Perspect 121:580–585. [PubMed: 23461877]

National Academy of Sciences (NAS) 2019. A Class Approach to Hazard Assessment of Organohalogen Flame Retardants. National Academies Press 2019, Washington , DC. 10.17226/25412

Patisaul HB, Roberts SC, Mabrey N, McCaffrey KA, Gear RB, Braun J, Belcher SM, and Stapleton HM. 2013. Accumulation and endocrine disrupting effects of the flame retardant mixture Firemaster(R) 550 in rats: an exploratory assessment. J Biochem Mol Toxicol 27: 124–136. [PubMed: 23139171]

Peng B, Yu ZM, Wu CC, Liu LY, Zeng L, and Zeng EY. 2020. Polybrominated diphenyl ethers and organophosphate esters flame retardants in play mats from China and the exposure risks for children. Environ Int 135:105348. [PubMed: 31884131]

Pfaffl MW. 2001.A new mathematical model for relative quantification in real-time RT-PCR. Nucl Acids Res. 29: e45. [PubMed: 11328886]

Pillai HK, Fang M, Beglov D, Kozakov D, Vajda S, Stapleton HM, Webster TF, and Schlezinger JJ. 2014. Ligand binding and activation of PPARγ by Firemaster® 550: effects on adipogenesis and osteogenesis in vitro. Environ Health Perspect 122:1225–1232. [PubMed: 25062436]

Sarruf DA, Yu F, Nguyen HT, Williams DL, Printz RL, Niswender KD, and Schwartz MW. 2009. Expression of peroxisome proliferator-activated receptor-gamma in key neuronal subsets regulating glucose metabolism and energy homeostasis. Endocrinology 150: 707–712. [PubMed: 18845632]

Schmittgen TD and Livak KJ.2008. Analyzing real-time PCR data by the comparative C(T) method. Nature Protoc. 3:1101–1108. [PubMed: 18546601]

Shen M, Senthil Kumar SPD, and Shi H. 2014. Estradiol regulates insulin signaling and inflammation in adipose tissue. Horm Mol Biol Clin Invest 17:99–107.

Shi X, Zhou F, Li X, Chang B, Li D, Wang Y, Tong Q, Xu Y, Fukuda M, Zhao JJ, Li D, Burrin DG, Chan L, and Guan X. 2013. Central GLP-2 enhances hepatic insulin sensitivity via activating PI3K signaling in POMC neurons. Cell Metab 18:86–98. [PubMed: 23823479]

Steves AN, Bradner JM, Fowler KL, Clarkson-Townsend D, Gill BJ, Turry AC, Caudle WM, Miller GW, Chan AWS, and Easley CA. 2018. Ubiquitous flame-retardant toxicants impair spermatogenesis in a human stem cell model. iScience 3:161–176. [PubMed: 29901031]

Stump M, Guo D-F, Lu K-T, Mukohda M, Liu X, Rahmouni K, and Sigmund CD. 2016. Effect of selective expression of dominant-negative PPARγ in pro-opiomelanocortin neurons on the control of energy balance. Physiol Genomics 48:491–501. [PubMed: 27199455]

Tung EWY, Ahmed S, Peshdary V, and Atlas E. 2017. Firemaster® 550 and its components isopropylated triphenyl phosphate and triphenyl phosphate enhance adipogenesis and transcriptional activity of peroxisome proliferator activated receptor (PPARγ) on the adipocyte protein 2 (aP2) promoter. PloS one 12 : e0175855–e0175855. [PubMed: 28437481]

van der Veen Ike, and de Boer Jacob. 2012. Phosphorus flame retardants: Properties, production, environmental occurrence, toxicity and analysis. Chemosphere 88:1119–1153. [PubMed: 22537891]

Vail GM, Walley SN, Yasrebi A, Maeng A, Conde KM, Roepke TA. 2020. The interactions of diet-induced obesity and organophosphate flame retardant exposure on energy homeostasis in adult male and female mice. J Toxicol Environ Health A 83: 438–455 [PubMed: 32546061]

Vail GM. And Roepke TA. 2020. Organophosphate flame retardants excite arcuate melanocortin circuitry and increase neuronal sensitivity to ghrelin in adult mice. Endocrinology 161(11):bqaa168 [PubMed: 32961558]

Wang Yong-Xu. 2010. PPARs: Diverse regulators in energy metabolism and metabolic diseases. Cell Res 20 :124–137. [PubMed: 20101262]

Wei GL, Li DQ Zhuo MN, Liao YS, Xie ZY, Guo TL, Li JJ, Zhang SY, and Liang ZQ. 2015. Organophosphate flame retardants and plasticizers: Sources, occurance, toxicity and human exposure. Environ Pollut 196: 29–46 [PubMed: 25290907]

Yang J, Zhao Y, Li M, Du M, Li X, and Li Y. 2019. A review of a class of emerging contaminants: The classification, distribution, intensity of consumption, dsynthesis routes, environmental effects and expectation of pollution abatement to organophosphate flame retardants (OPFRs). Int J Mol Sci 20:2874–2912.

Yasin S, Behary N, Curti M, and Rovero G. 2016. Global consumption of flame retardants and related environmental concerns: A study on possible mechanical recycling of flame retardant textiles. FIBER 4:16.

Yasrebi A, Hsieh A, Mamounis KJ, Krumm EA, Yang JA, Magby J, Pu H, and Roepke TA. 2016. Differntial gene regulation of GHSR signaling pathway in the arcuate nucleus and NPY neuros by fasting, diet-induced obestiy, and 17b-estradiol. Mol Endocrinol 422:42–56.

Young AS, Allen JG, Kim UJ, Seller S, Webster TF, Kannan K, and Ceballos DM. 2018. Phthalate and organophosphate plasticizers in nail polish: Evaluation of labels and ingredients. Environ Sci Technol 52:12841–12850. [PubMed: 30302996]

Zota AR, Linderholm L, Park JS, Petreas M, Guo T, Privalsky ML, Zoeller RT, and Woodruff TJ. 2013. Temporal comparison of PBDEs, OH-PBDEs, PCBs, and OH-PCBs in the serum of second trimester pregnant women recruited from San Francisco General Hospital, California. Environ Sci Technol 47:11776–11784. [PubMed: 24066858]

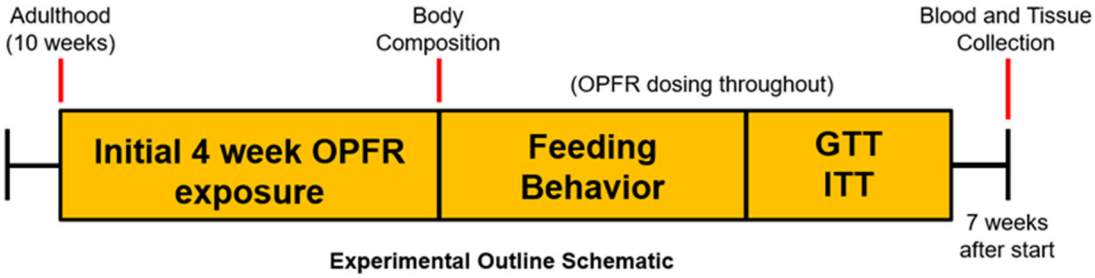

Figure 1.

Experimental timeline graphic. OPFR- and control-oil dosing began at 10 weeks of age and continued for the entire duration of experiments. At this time initial bodyweight and body composition data were acquired. During the first 4 weeks, bodyweight and crude food intake were measured weekly. After 4 weeks body composition was measured again. Next, feeding behavior was analyzed, followed by glucose and insulin tolerance tests. After recovery from tolerance tests, animals were euthanized for tissue and blood collection.

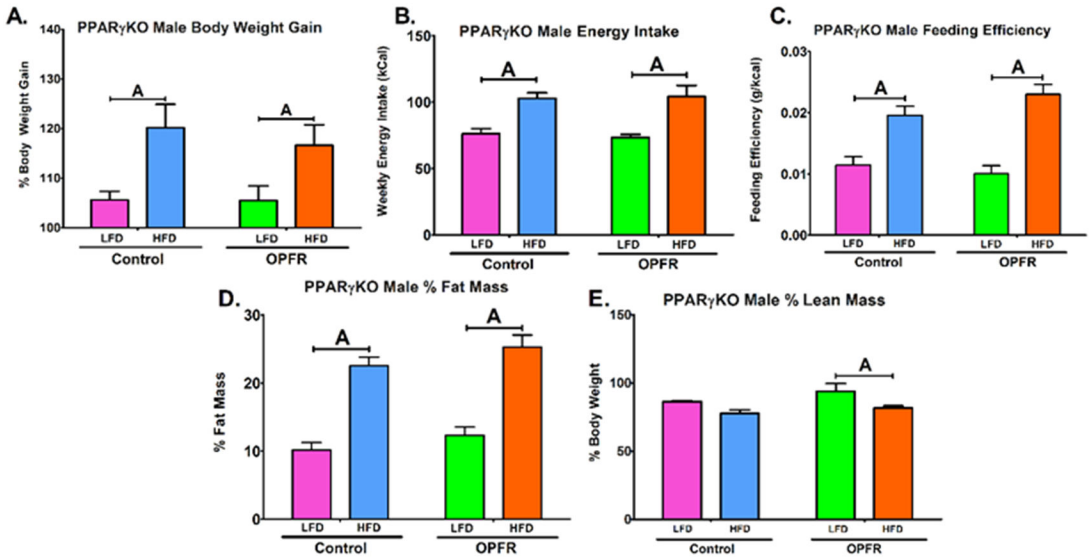

Figure 2.

Physiological parameters in neuron-specific PPARγKO males orally dosed with an OPFR mixture (1 mg/kg bw) for 4 weeks. **(A)** % Body Weight Gain over 4 weeks; **(B)** Energy Intake; **(C)** Feeding Efficiency; **(D)** Body composition % Fat Mass; **(E)** Body composition % Lean Mass. Data were analyzed by a two-way ANOVA with post-hoc Newman-Keul's multiple comparisons test. Uppercase letters denote diet effects within exposure group. Lowercase letters denote OPFR effects within diet group. Data (A, D, E n=6-8 animals; B, C n=4 pairhoused cages) are presented as mean ± SEM.

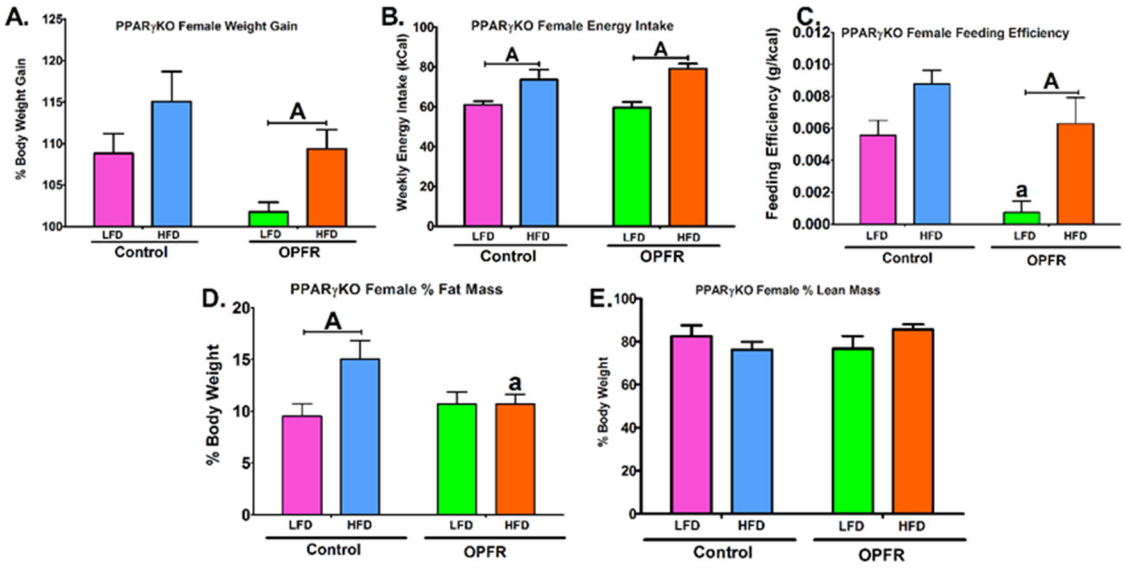

Figure 3.

Physiological parameters in nueron-specific PPARγKO females orally dosed with an OPFR mixture (1 mg/kg bw) for 4 weeks. **(A)** % Body Weight Gain over 4 weeks; **(B)** Energy Intake; **(C)** Feeding Efficiency; **(D)** Body composition % Fat Mass; **(E)** Body composition % Lean Mass. Data were analyzed by a two-way ANOVA with post-hoc Newman-Keul's multiple comparisons test. Uppercase letters denote diet effects within exposure group. Lowercase letters denote OPFR effects within diet group. Data (A, D, E n=6-8 animals; B, C n=4 pairhoused cages) are presented as mean ± SEM.

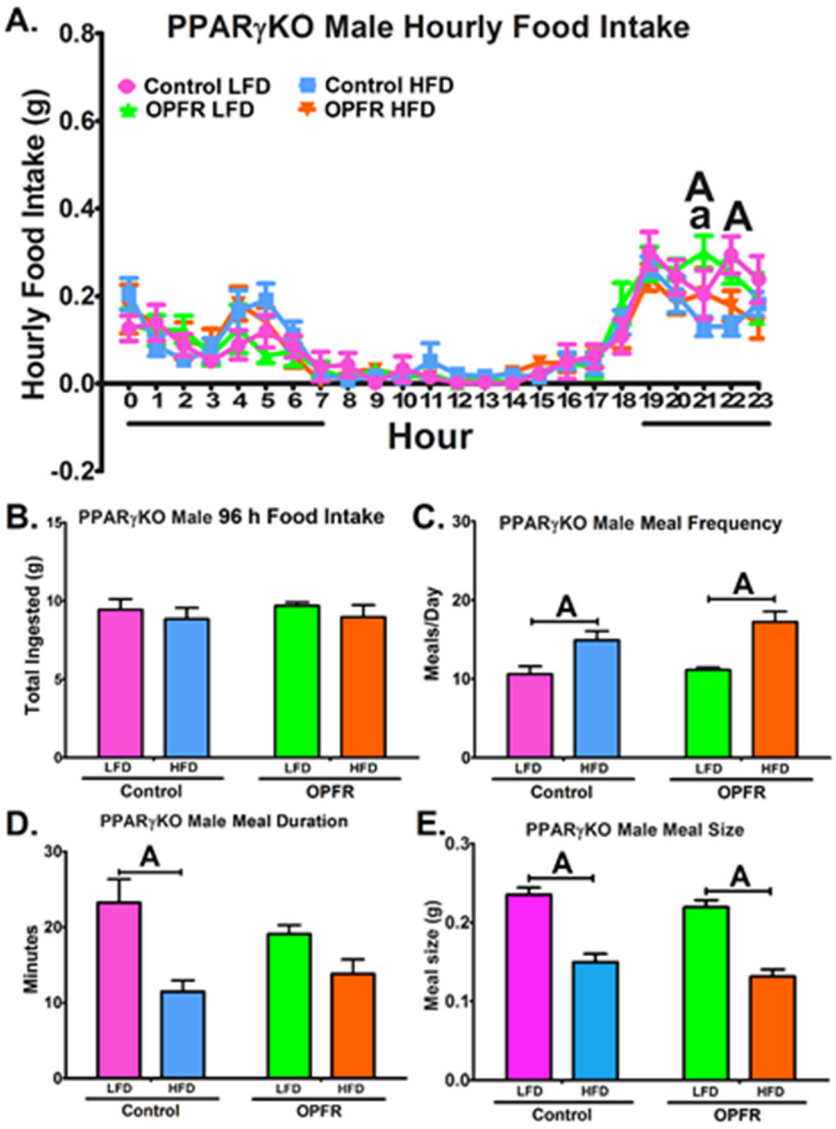

Figure 4.

Analysis of feeding behaviors in neuron-specific PPARγKO males orally dosed with an OPFR mixture (1 mg/kg bw) for ~5 weeks. **(A)** hourly food intake; **(B)** 96 h total food ingested **(C)** meals/day; **(D)** meal duration; **(E)** meal size. Data were analyzed by a two-way ANOVA (B-E) and a repeated-measures three-way ANOVA (A) with post-hoc Newman-Keul's test. Uppercase letters denote diet effects within exposure group; and lowercase letters denote OPFR effects within diet group. Data (n=6-8 for all groups) are presented as mean ± SEM.

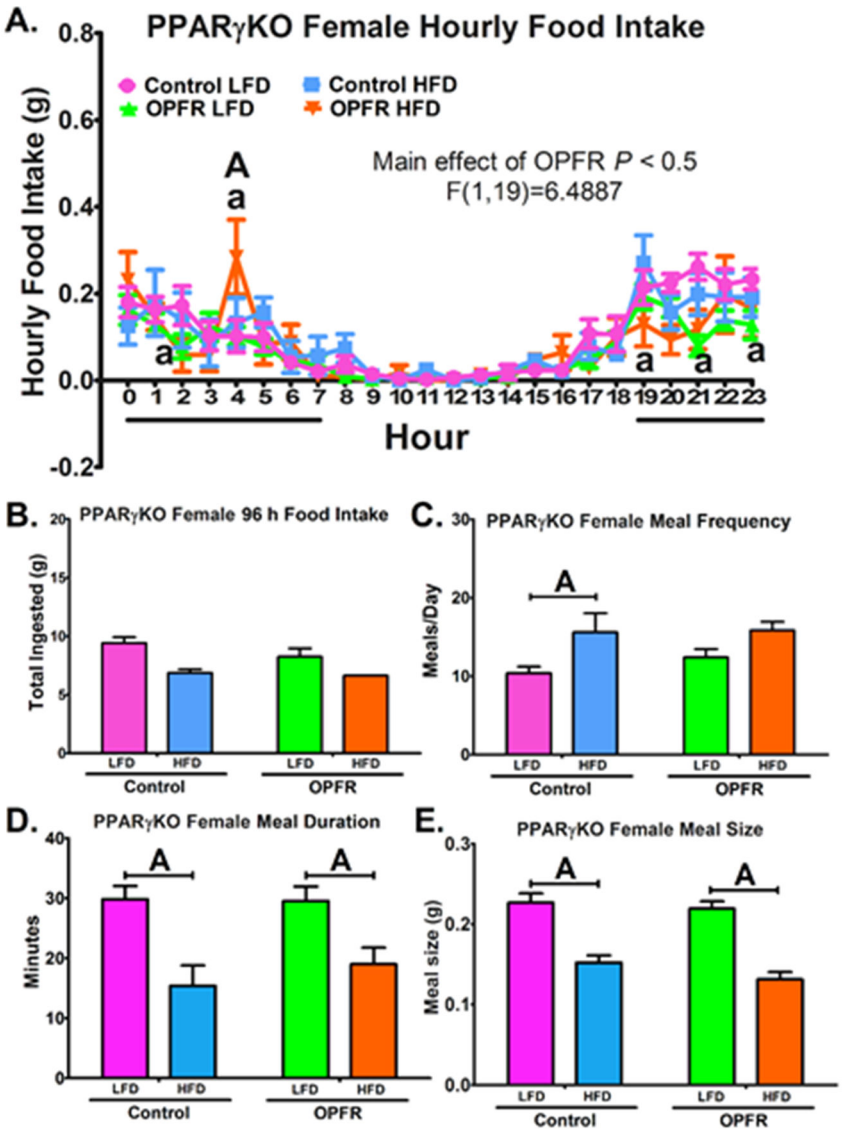

Figure 5.

Analysis of feeding behaviors in neuron-specific PPARγKO females orally dosed with an OPFR mixture (1 mg/kg bw) for ~5 weeks. **(A)** hourly food intake; **(B)** 96 h total food ingested **(C)** meals/day; **(D)** meal duration; **(E)** meal size. Data were analyzed by a two-way ANOVA (B-E) and a repeated-measures three-way ANOVA (A) with post-hoc Newman-Keul's test. Uppercase letters denote diet effects within exposure group; and lowercase letters denote OPFR effects within diet group. Data (n=4-7 for all groups, excepting (B) which exhibited excessive food chewing reducing usable data to n=1 and n=2 for control and OPFR HFD, respectively) are presented as mean ± SEM.

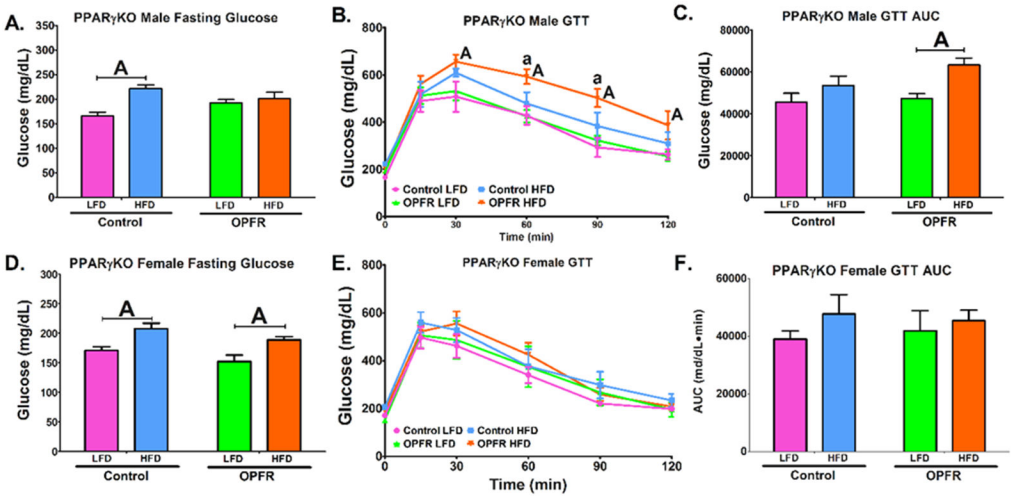

Figure 6.

Glucose tolerance tests in neuron-specific PPARγKO mice orally dosed with an OPFR mixture (1 mg/kg bw) for ~6 weeks. **(A)** Male fasting glucose; **(B)** Male GTT; **(C)** Area under the curve (AUC) of Male GTT; **(D)** Female fasting glucose; **(E)** Female GTT; **(F)** Area under the curve (AUC) of Female GTT. Data were analyzed by a two-way ANOVA (A, C, D, F) or a repeated-measures, three-way ANOVA (B, E) with post-hoc Newman-Keul's multiple comparisons test. Uppercase letters denote diet effects within exposure group and lowercase letters denote OPFR effect within diet group. Data (n=5-8 for all groups) are presented as mean ± SEM.

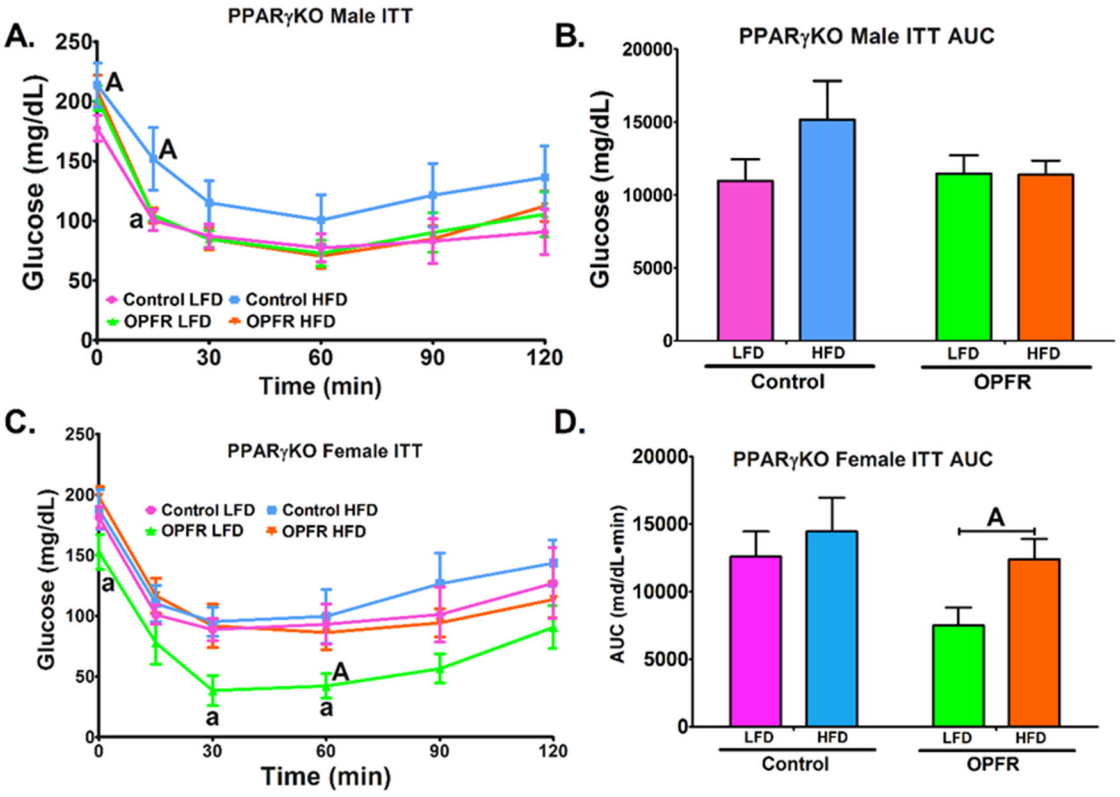

Figure 7.

Insulin tolerance tests in neuron-specific PPARγKO mice orally dosed with an OPFR mixture (1 mg/kg bw) for ~6 weeks. **(A)** Male ITT; **(B)** Area under the curve (AUC) of Male ITT; **(C)** Female GTT; **(D)** Area under the curve (AUC) of Female ITT. Data were analyzed by a two-way ANOVA (B,D) or a repeated-measures, three-way ANOVA (A, C) with post-hoc Newman-Keul's multiple comparisons test. Uppercase letters denote diet effects within exposure group and lowercase letters denote OPFR effect within diet group. Data (n=5-8 for all groups) are presented as mean ± SEM.

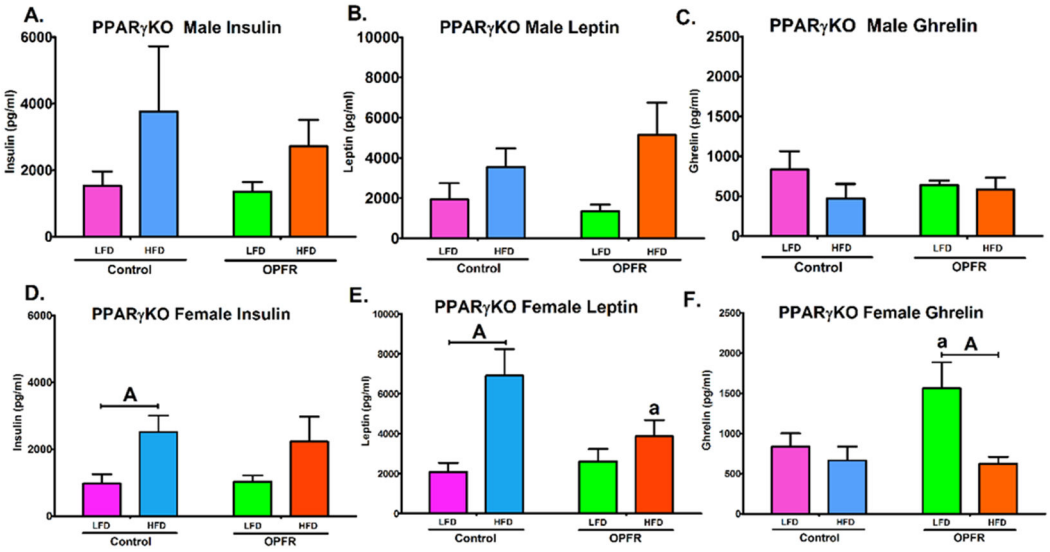

Figure 8.

Terminal plasma peptide hormone levels in neuron-specific PPARγKO mice orally dosed with an OPFR mixture (1 mg/kg bw) for ~7 weeks. **(A)** Male insulin; **(B)** Male leptin; **(C)** Male ghrelin; **(D)** Female insulin; **(E)** Female leptin; **(F)** Female ghrelin. Data were analyzed by a two-way ANOVA (B,D) or a repeated-measures, three-way ANOVA (A, C) with post-hoc Newman-Keul's multiple comparisons test. Uppercase letters denote diet effects within exposure group and lowercase letters denote OPFR effect within diet group. Data (n=6-8 for all groups) are presented as mean ± SEM.

Table 1.
List of primer pairs for real-time quantitative PCR

Reference genes: *Actβ, Gapdh, Hprt. Actβ* = β-actin; *Agrp* = agouti-related peptide; *Cart* = cocaine- and amphetamine-regulated transcript; *Npy* = neuropeptide Y; *Pomc* = proopiomelanocortin; Gapdh = glyceraldehyde-3-phosphate dehydrogenase; Ghsr = growth hormone secretagogue receptor (ghrelin receptor); *Hprt* = hypoxanthine-guanine phosphoribosyltransferase; *Insr* = insulin receptor; *Lepr* = leptin receptor; *Esr1* = estrogen receptor 1 (ERα).

Gene Name	Product Length	Primer Eff. (%)	Primer sequence	Base Pair #	Accession #
Actβ	63	101	F:GCCCTGAGGCTCTTTTCCA R:TAGTTTCATGGATGCCACAGGA	849-867 890-911	NM_007393.3
Agrp	146	105	F:CTCCACTGAAGGGCATCAGAA R:ATCTAGCACCTCCGCCAAA	287-307 414-432	NM_007427.2
Cart	169	95	F:GCTCAAGAGTAAACGCATTCC R:GTCCCTTCACAAGCACTTCAA	227-297 425-445	NM_013732
Gapdh	98	93	F:TGACGTGCCGCCTGGAGAAA R:AGTGTAGCCCAAGATGCCCTTCAG	778-797 852-875	NM_008084.2
Ghsr	122	123	F:CAGGGACCAGAACCACAAAC R:AGCCAGGCTCGAAAGACT	1003-1022 1107-1124	NM_177330
Hprt	117	107	F:GCTTGCTGGTGAAAAGGACCTCTCGAAG R:CCCTGAAGTACTCATTATAGTCAAGGGCAT	631-658 718-747	NM_013556
Insr	89	114	F: GTGTTCGGAACCTGATGAC R: GTGATACCAGAGCATAGGAG	1215-1233 1686-1706	NM_010568
Lepr	149	105	F:AGAATGACGCAGGGCTGTAT R:TCCTTGTGCCCAGGAACAAT	3056-3075 3185-3204	NM_146146.2
Npy	182	100	F:ACTGACCCTCGCTCTATCTC R:TCTCAGGGCTGGATCTCTTG	106-125 268-287	NM_023456
Pomc	200	103	F:GGAAGATGCCGAGATTCTGC R:TCCGTTGCCAGGAAACAC	145-164 327-344	NM_008895
Esr1	113	115	F:AATGTCCACCCGCTAGGCATTC R:CTCCATGTCTTGCGTAGGTCTC	298-319 389-410	NM_010157

Table 2.

Arcuate expression of neuropeptides and receptors from PPARγKO males and females.

Data were analyzed by a two-way ANOVA with post-hoc Newman-Keuls multiple comparisons test. Uppercase letters denote diet effects within OPFR group and lowercase letters denote OPFR effect within diet. All data were normalized to Control-LFD within each sex. Data (n = 5-6 per group) are presented as mean ± SEM. Significant overall ANOVA effects are as follows. **Male**: *Agrp* $F(1,7)_{Diet}$= 11.33, P < .05; *Cart* $F(1,17)_{Diet}$= 4.984, P < .05; *Npy* $F(1,17)_{Diet}$= 5.057, P < .05. **Female**: *Agrp* $F(1,19)_{Diet}$= 22.93, P = .05; *Npy* $F(1,19)_{Diet}$= 16.93, P <.05; *Ghsr* $F(1,19)_{OPFR}$= 6.601, P < .05.

	Males				Females			
Gene	**Control-LFD**	**Control-HFD**	**OPFR-LFD**	**OPFR-HFD**	**Control-LFD**	**Control-HFD**	**OPFR-LFD**	**OPFR-HFD**
Agrp	1.05 ± 0.17	**0.51 ± 0.10A**	0.77 ± 0.11	0.46 ± 0.11	1.09 ± 0.19	**0.52 ± 0.11A**	1.41 ± 0.17	**0.55 ± 0.08A**
Cart	1.02 ± 0.10	1.33 ± 0.14	1.02 ± 0.08	1.19 ± 0.10	1.01 ± 0.06	0.99 ± 0.11	0.76 ± 0.08	1.03 ± 0.17
Esr1	1.05 ± 0.15	1.09 ± 0.11	1.17 ± 0.06	1.10 ± 0.08	1.02 ± 0.08	0.92 ± 0.06	1.20 ± 0.15	1.12 ± 0.10
Npy	1.05 ± 0.16	0.69 ± 0.11	0.94 ± 0.11	0.70 ± 0.16	1.03 ± 0.11	**0.60 ± 0.05A**	1.32 ± 0.11	**0.74 ± 0.10A**
Ghsr	1.07 ± 0.21	1.01 ± 0.12	1.01 ± 0.10	0.93 ± 0.08	1.02 ± 0.09	0.80 ± 0.13	**0.73 ± 0.03a**	0.66 ± 0.06
Insr	1.01 ± 0.06	1.08 ± 0.15	1.02 ± 0.07	1.24 ± 0.16	1.02 ± 0.10	1.09 ± 0.10	1.00 ± 0.12	1.04 ± 0.16
Lepr	1.05 ± 0.17	1.00 ± 0.13	1.04 ± 0.09	1.01 ± 0.09	1.01 ± 0.05	0.66 ± 0.04	1.04 ± 0.10	1.03 ± 0.15
Esr1	1.02 ± 0.09	1.16 ± 0.17	0.80 ± 0.04	1.02 ± 0.10	1.04 ± 0.12	1.09 ± 0.09	0.82 ± 0.15	1.12 ± 0.13

Table 3.
Summary of PPARγKO findings compared to WT findings by Vail et al. (2020a)

Only parameters measured in both studies are presented. Up arrows denote an OPFR-induced increase and down arrows denote an OPFR-induced decrease. One up and one down arrow indicates a mixed effect dependent on time of day. N.S. = not significant.

Endpoint	Males		Females	
	LFD	HFD	LFD	HFD
	WT / PPARγKO	WT / PPARγKO	WT / PPARγKO	WT / PPARγKO
Bodyweight Gain	n.s. / n.s.	↑ / n.s.	n.s. / n.s.	n.s. / n.s.
Feeding Efficiency	n.s. / n.s.	n.s. / n.s.	n.s. / ↓	n.s. / n.s.
Fat Mass	n.s. / n.s.	↑ / n.s.	n.s. / ↓	n.s. / n.s.
Lean Mass	n.s. / n.s.	↓ / n.s.	n.s. / n.s.	n.s. / n.s.
96 h Food Intake	n.s. / n.s.	n.s. / n.s.	n.s. / n.s.	↓ / n.s.
Hourly Food Intake	n.s. / n.s.	↓↑ / n.s.	n.s. / ↓↑	↓↑ / ↓↑
Meal Frequency	n.s. / n.s.	n.s. / n.s.	n.s. / n.s.	↓ / n.s.
Meal Duration	n.s. / n.s.	n.s. / n.s.	n.s. / n.s.	n.s. / n.s.
Meal Size	n.s. / n.s.	n.s. / n.s.	n.s. / n.s.	n.s. / n.s.
Fasting Glucose	n.s. / n.s.	n.s. / n.s.	n.s. / n.s.	n.s. / n.s.
Glucose Tolerance	n.s. / n.s.	n.s. / ↓	n.s. / n.s.	n.s. / n.s.
Insulin Tolerance	n.s. / n.s.	n.s. / n.s.	n.s. / ↓	n.s. / n.s.
Plasma Insulin	n.s. / n.s.	n.s. / n.s.	↑ / n.s.	n.s. / n.s.
Plasma Leptin	n.s. / n.s.	n.s. / n.s.	n.s. / n.s.	↑ / ↓
Plasma Ghrelin	↓ / n.s.	n.s. / n.s.	n.s. / ↑	n.s. / n.s.